Effects of Bending and Bending Angular Momentum on Reaction of NO_2^+ with C_2H_2: A Quasi-Classical Trajectory Study†

Jason M. Boyle,‡ Jianbo Liu,§ and Scott L. Anderson*,‡

Department of Chemistry, University of Utah, 315 S. 1400 E. Rm 2020, Salt Lake City, Utah 84112, and Department of Chemistry and Biochemistry, Queens College of CUNY, 65-30 Kissena Boulevard, Flushing, New York 11367

Received: November 18, 2008; Revised Manuscript Received: December 18, 2008

A large set of quasi-classical trajectories were calculated at the PBE1PBE/6-311G** level of theory, in an attempt to understand the mechanistic origins of the large, mode-specific enhancement of the O-transfer reaction by NO_2^+ bending vibration and the surprisingly large suppressing effect of bending angular momentum. The trajectories reproduce the magnitude of the absolute reaction cross section, and also get the dependence of reactivity on NO_2^+ vibrational state, and the vibrational state dependent scattering behavior qualitatively correct. Analysis of the trajectories shows that the bending effect is not simply a consequence of enhanced reactivity in bent geometries but, rather, that excitation of bending motion allows reaction in a wider range of orientation angles, even if the NO_2^+ is not bent at the onset of the collisional interaction. There is a strong interplay between NO_2^+ bending and transient charge transfer during the collisions. Such charge transfer enhances reactivity, but only if the reactants are oriented correctly.

I. Introduction

Recently, we reported an experimental study of vibrational mode and collision energy effects on the dynamics of oxygen transfer in the $NO_2^+ + C_2H_2$ reaction.[1] The dynamics of this apparently simple reaction proved to be surprisingly complex, with several features that could not be rationalized on the basis of the experimental results, including RRKM analysis of an ab initio reaction coordinate. Here, we report a quasi-classical trajectory (QCT) study of $NO_2^+ + C_2H_2$ collisions, aimed at understanding the following key features of this system at high collision energies: (1) the severe bottleneck to this atom-transfer reaction; (2) the strong vibrational enhancement, particularly from NO_2^+ bending; (3) the strong suppressing effect of bending angular momentum; (4) the mechanism by which bend excitation influences the product recoil dynamics. Before describing the QCT methodology and results, we first outline the key features of the reaction coordinate and experimental results.

II. Summary of the Experimental Results and Properties of the System

An ab initio reaction coordinate, calculated at the B3LYP/6-311++G** level of theory, is shown in Figure 1. The two product channels, $NO^+ + H_2CCO$ and $NO + H_2CCO^+$, represent two different, nearly isoenergetic, electronic states of $(NO + \text{ketene})^+$. The two channels show virtually identical dynamics, including dependence on collision energy and reactant vibrational excitation, as well as product recoil behavior. The reason is clear in Figure 1. The reaction coordinate bifurcates into the two product channels quite late in the collision, as the products separate, and the charge has to localize on one or the other. Mulliken charge calculations indicate that the charge is delocalized in all of the complexes and TSs of interest during the collision. Properties such as vibrational state or collision energy dependences can only depend on dynamics leading up to the rate-limiting step on the reaction coordinate, which in this case occurs early in the collisions (see below). Recoil behavior, of course, will depend on dynamics throughout the course of the collisions; however, the gross features of the scattering (stripping vs rebound dynamics, energy disposal) are apparently only weakly dependent on dynamics occurring during product separation. For the purposes of this paper we, therefore, focus on the factors controlling total reactivity, i.e., on dynamics leading up to the rate-limiting step. Early time dynamics are ideal for quasi-classical trajectories, because error tends to be cumulative during a trajectory (see below) and because the method is not amenable to studying the process of branching into two product states.

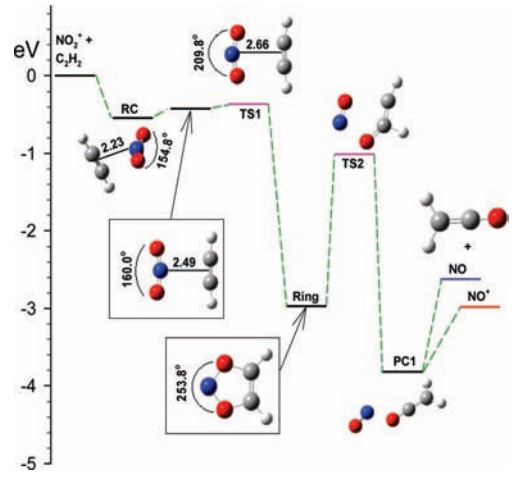

Figure 1. Reaction coordinate connecting NO_2^+ and C_2H_2 reactants to the two charge states of the $[NO + \text{ketene}]^+$ products. Distances labeled in inset images are in angstroms.

The experimental reactivity results are summarized in Figure 2a, which gives the collision energy ("E_{col}", center-of-mass frame) dependence of the total cross section (σ_{Total}), and Figure

† Part of the "George C. Schatz Festschrift".
‡ Department of Chemistry, University of Utah.
§ Department of Chemistry and Biochemistry, Queens College of CUNY.

10.1021/jp8101404 CCC: $40.75
Published on Web 01/30/2009

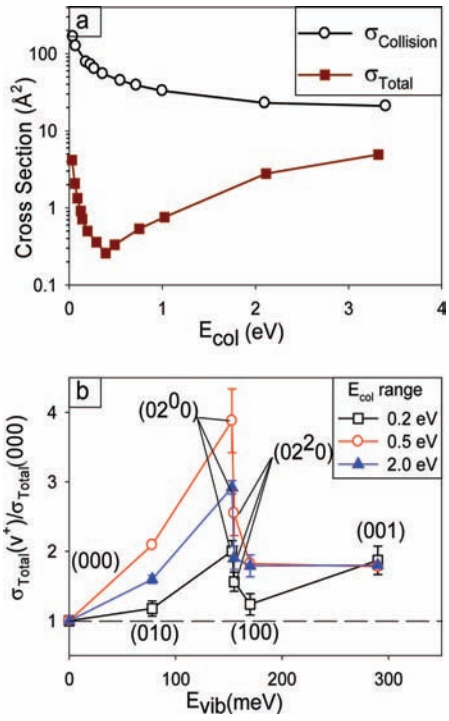

Figure 2. (a) Comparison of the collision cross section and the experimental total cross section for reaction of ground-state NO_2^+ with C_2H_2 as a function of collision energy. (b) Vibrational enhancements factors, $\sigma(n_1n_2n_3)/\sigma(000)$ in three collision energy ranges. Error bars are the standard deviations of data taken on separate days.

2b, which plots the effect on reactivity of exciting the various NO_2^+ vibrational states, as a function of the vibrational state energy (E_{vib}) for several ranges of E_{col}. To show the vibrational effects more clearly, Figure 2b gives ratios of the cross section for reaction of vibrationally excited NO_2^+ to the ground-state cross section: $\sigma_{Total}(n_1n_2n_3)/\sigma_{Total}(000)$. The notation $(n_1n_2n_3)$ gives the number of quanta excited in the symmetric stretch, bend, and asymmetric stretch modes, respectively. The x-axis of Figure 2b gives the vibrational state energies.

Note (Figure 2a) that the cross section has strong bimodal dependence on E_{col} and is substantially smaller than the collision cross section, which is taken as the larger of the ion-induced dipole capture cross section and hard sphere cross sections. Clearly there is a bottleneck inhibiting this barrierless, exoergic reaction, and RRKM analysis of the various complexes and transition states on the reaction coordinate suggests that the bottleneck (at least for low E_{col}) is TS1.[1] The bottleneck was attributed to TS1 being tight, i.e., the energy increases rapidly for distortion away from the C_{2v} symmetry TS1 geometry. The spike in reactivity at low E_{col} was attributed to mediation by the weakly bound complex "RC", allowing the system time to find its way to the TS1 geometry. At high E_{col}, the cross section increases because there is enough energy to react in nonoptimal geometries, although σ_{Total} remains well below $\sigma_{collision}$. At E_{col} near 0.5 eV, the RC lifetime is too short to mediate reaction, but the available energy is still too low to significantly loosen the geometric requirement for reaction; thus reaction occurs only in the small fraction (<1%) of collisions that occur near the ideal TS1 geometry.

All modes of NO_2^+ vibration enhance reaction (Figure 2b) at all collision energies, even at low E_{col} where collision energy inhibits reaction. At high E_{col}, where both E_{col} and E_{vib} enhance reaction, asymmetric stretch (001) excitation has an enhancing effect roughly 3 times larger than the effect of adding an equivalent amount of E_{col} (0.29 eV). Enhancement from this mode is not surprising—asymmetric ON−O stretching should be the mode most strongly coupled to the reaction coordinate for oxygen transfer. The other modes give even larger enhancements, however. Symmetric stretch (100) excitation is about 5 times more effective than the equivalent amount (0.17 eV) of E_{col}, and bending excitation is up to 16 more efficient. The bend enhancements are, however, strongly dependent on whether there is angular momentum associated with the bending motion. Compare the effects of the two bend overtone states: (02^00) with E_{vib} = 153 meV, and (02^20) with E_{vib} = 155 meV, where the 0 or 2 superscript refers to the angular momentum associated with bending. The (02^00) state gives rise to approximately twice the enhancement seen for the (010) state, as might be expected; however, (02^20) excitation is considerably less effective (but still more effective than either stretch vibration). The difference in both energy and angular momentum between the (02^00) and (02^20) states is negligible compared to the energy and angular momentum of the collisions; thus the reactivity difference must reflect a difference in the nature of the reactant motion. This is, by far, the largest effect of bending angular momentum on reactivity ever observed,[2−6] and elucidating the mechanism is one of the main goals of the QCT study.

Another unusual feature of this reaction is that the pattern of vibrational mode effects is constant over a wide range of E_{col}, even though the reaction mechanism clearly changes from complex-mediated (E_{col} < ~0.4 eV) to direct (E_{col} > ~1 eV). Over the same E_{col} range the time scale of the collisions decreases from being many times the vibrational time scale to being comparable. The magnitude of the vibrational effects remains large, even at high E_{col} where the E_{vib} is only a few percent of the total reactant energy.

Finally, the experimental study found that NO_2^+ vibrational excitation, particular bending, results in substantial changes in the product recoil dynamics at high collision energies, leading to a more forward-scattered velocity distribution than for the ground state. In past studies of vibrational effects on product recoil in ion reactions, we have seen insignificant effects on product recoil, even for reactions where vibration strongly affects reactivity.[5,7−17] Lack of vibrational effects on recoil is not surprising—energy is likely to be scrambled in reactive collisions, and reactant E_{vib} is typically only a small fraction of the total energy available to products, particularly at high E_{col}. As might be expected, the exception has been for endoergic reactions near threshold, where E_{vib} ***is*** a significant fraction of the energy available to products.[14,18] The present reaction is more than 2.5 eV exoergic, such that the bending vibrations contribute <3.5% of the available energy at high E_{col}.

III. Computational Methodology

Quasi-classical, direct dynamics trajectories were calculated for a collision energy of 2 eV, and for NO_2^+ in its ground, (02^00), and (02^20) states. The QCT method is not suitable for low-energy collisions, both because the trajectory time scale is unfeasibly long and because errors arising from treating vibration classically become severe (see below). The method used to calculate quasi-classical initial conditions for states including vibrational angular momentum and ZPE was discussed in detail by Lourderaj et al.[19] The quasi-classical initial vibrational state is simulated by giving the reactant atoms displacements from equilibrium and kinetic energies appropriate to the desired initial rovibrational state, with random phases for the different modes, and random initial orientations. Because the experiments generated NO_2^+ by REMPI of a supersonic molecular beam, a 50 K

Boltzmann distribution was sampled to select the NO_2^+ initial rotational state. The NO_2^+ vibrational state included the desired mode-selective vibrational excitation plus zero-point energy (ZPE) in all modes. The C_2H_2 in the experiments was at room temperature, thus the trajectory initial state included ZPE for all vibrational modes, and a rotational state sampled from a 300 K Boltzmann distribution. The VENUS program of Hase and co-workers[20] was used to calculate initial atomic positions and velocities, and trajectories were integrated using the updating Hessian method of Schlegel and co-workers,[21] implemented in GAUSSIAN03.[22]

In order to get statistics good enough to examine vibrational effects for a reaction with small cross section, thousands of trajectories are required, and we try to use theoretical methods that require less than ~12 CPU hours/trajectory. Candidate methods and basis sets were benchmarked against single point calculations at the QCISD(T)/cc-pVTZ level of theory. Following the approach we have used successfully for several other ion−molecule systems,[5,23−25] we initially tested how well each method reproduced benchmark energies for approach of NO_2^+ to C_2H_2 and for important stationary points on the reaction coordinate, leading up to the rate-limiting point (TS1). This process led to selection of the MP2/6-31G* method for the initial set of trajectories; however, the calculated reaction cross sections were much smaller than the experimental cross sections and failed to reproduce the observed vibrational effects. The reason is that while MP2/6-31G* reproduces benchmark energies for reactant approach in several symmetric geometries, and also the complex and TS1 energies, it overestimates energies of nonsymmetric points near TS1; i.e., the critical TS is too tight at the MP2/6-31G* level. Conversely, B3LYP/6-31G* results in an overly loose TS1, such that the calculated reaction efficiency is nearly unity independent of vibrational state.

Clearly it is critical to identify a level of theory that reasonably represents the regions of the potential surface that the trajectories actually explore as they approach the rate-limiting step in the reaction. For this purpose, we took several reactive and nonreactive trajectories calculated at the MP2/6-31G* and B3LYP/6-31G* levels and selected six geometries corresponding to points where bonds appeared to be breaking or forming in various reactant orientations. A variety of levels of theory were then compared to QCISD(T)/cc-pVTZ energies at these selected geometries. On the basis of the overall level of agreement and computational speed, we chose the PBE1PBE/6-311G** level of theory for the main set of trajectories. At this level of theory, each trajectory takes ~22 CPU hours on our Athlon 64-based cluster, forcing us to limit the scope of the calculations.

Trajectories were calculated for only one collision energy (2 eV) and for the three reactant states of greatest interest (ground state, (02^00), and (02^20)). Because the number of trajectories was necessarily limited, we adopted the following strategy in order to minimize the uncertainty in comparing behavior for different NO_2^+ states or impact parameters. For each state, batches of trajectories (typically 300) were calculated for discrete values of the reactant impact parameter (b = 1, 1.5, 2, 2.5 Å) rather than randomly sampling the b distribution. Collisions at impact parameters below 1 Å were omitted because their weighting in the integral cross section is small, and only 60 trajectories were calculated for each state at b = 2.5 Å because no reaction was observed.

In addition, the random number generator seed used in setting up initial conditions for each batch of trajectories was identical. Each trajectory batch, therefore, used the same pseudorandom sequence to sample the reactant parameter space (orientations, rotational energies, rotational and vibrational phases, etc.). The main motivation for this pseudorandom sampling procedure was to avoid a potentially serious problem that arises when reactivity is sharply dependent on one or more reactant parameters. For example, in our previous studies of H_2CO^+ reactions with CD_4 and D_2,[23,24] reactivity was found to be highly sensitive to orientation. As a result, when trajectory batches for different reactant states (for example) were calculated with random sampling of the initial conditions, the slightly different distributions of orientation in different batches resulted in variations in reaction probability that were comparable to the effects of reactant state. By use of the same pseudorandom sequence for each batch, the error from inadequate sampling of reactant parameter space is the same for all batches and tends to cancel when comparing batches for different states or impact parameters. A secondary benefit is that trajectories for different NO_2^+ states or impact parameters can be compared directly, because corresponding trajectories from different batches have identical initial conditions, apart from the parameter being varied (i.e., the NO_2^+ state or impact parameter).

Trajectory integration was performed with a step size of 0.25 amu$^{1/2}$ bohr (~0.56 fs), and trajectories were terminated either when the distance between the final products exceeded 9.0 Å or after 500 steps. To minimize time spent calculating the reactant approach phase of the trajectories, they were started at an initial inter-reactant separation of 7 Å. At this distance, the long-range ion-induced dipole interaction is not negligible. Using the angle-averaged polarizability of acetylene,[26] we can estimate that the potential is ~12 meV at 7 Å. This means that if the trajectories had been started at infinite separation, the collision energy would have been increased by ~12 meV by the 7 Å separation. In effect, by starting the trajectories at 7 Å with a relative energy of 2 eV, we effectively are simulating collisions at 1.988 eV collision energy. This shift from the 2 eV nominal energy is insignificant compared to the 0.38 eV collision energy spread in the experiments, which results from both the energy distribution of the primary beam (0.15 eV) and Doppler broadening from thermal motion of the acetylene target.[27] Energy conservation was better than 0.01 eV for all trajectories. The analysis below is based on a total ~2900 trajectories, corresponding to ~6.8 years of Athlon 64 CPU time.

Because trajectories were calculated at discrete b values, the trajectory cross sections were estimated using an extended closed trapezoidal approximation[28] to the usual integral form, where $P(b)$ is the fraction of reactive trajectories at each impact parameter, i.e., the opacity function

$$\sigma = 2\pi\int_0^{b_{max}} P(b)b\,db \approx \pi\sum_{b_i=0}^{b_{max}} [P(b_i)b_i + P(b_{i+1})b_{i+1}](b_{i+1} - b_i)$$

For trajectory visualization we use the program gOpenMol.[29] Detailed analysis of individual trajectories and statistical analysis of the trajectory ensemble were done with programs written for this purpose,[25] available from the corresponding author upon request.

Potential Problems with QCT. There are several issues with using the QCT method to probe vibrational dynamics in systems like $NO_2^+ + C_2H_2$. One obvious point is that vibration is not quantized, leading to several types of nonphysical behavior. At the start of the trajectories, the vibrational energy is partitioned appropriately to represent the classical analogue of the desired initial quantum state. During the time required for reactant

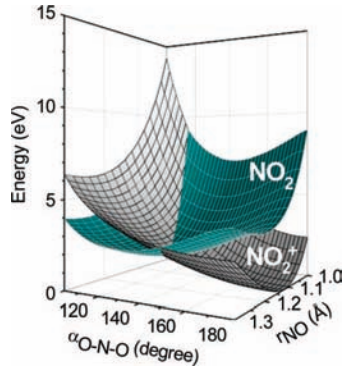

Figure 3. Cut through the potential energy surfaces for the $(NO_2 + C_2H_2)^+$ system along the NO_2 bend and symmetric stretch coordinates, at infinite reactant separation.

approach, the initial energy partitioning can decay via anharmonic coupling of the normal modes, such that the vibrational motion at the moment of collision no longer represents the state of interest. Several factors help minimize this issue for the present system. The collision energy is high, and we start the trajectories with reactant center-of-mass separation of only 7 Å, so that only ~100 fs elapse prior to the collision. Because both reactants are small molecules, the number of symmetry-allowed mode combinations capable of coupling to the initial state is limited.

It is easy to check for decay of the initial vibrational state by simply monitoring the vibrational amplitudes of various molecular geometric parameters as the reactants approach each other. For example, perhaps the most likely combination for intermode energy transfer is $(02^00) \leftrightarrow (100)$, because these two states have the same symmetry and similar frequencies (the quantum states are in Fermi resonance with ~10% mixing of the zeroth order stretch and bend overtone levels). If the initial (02^00) excitation decayed during reactant approach, this would be obvious as a decrease in the amplitude of the NO_2^+ bending motion, with corresponding amplitude increase in some other mode, such as the symmetric stretch. As can be seen in the trajectory plots discussed below, the amplitudes are quite constant up to the point where collisional interaction begins to perturb the motion. In fact, we see little change in amplitudes even in noncolliding test trajectories where the total time monitored is 5 times longer than the typical reactant approach. We conclude that at the "moment of collision", the trajectories still represent the desired states, at least to the extent possible in the quasi-classical framework.

Lack of quantization presumably has a significant effect on how energy is distributed between vibrational modes during and after collisions.[30,31] Here again, the fact that we are interested in high E_{col} helps, in that the available energy is large compared to the vibrational quanta, reducing the error associated with treating the motion classically. More importantly, the observables of greatest interest for our purposes are the effects of NO_2^+ vibration on the cross section, which depend only on dynamics up to the rate-limiting point on the reaction coordinate. The experimental observation of strong, mode-specific vibrational effects indicates that the rate-limiting point must be early in the collision, before the initial excitation is scrambled. Such systems are ideal for QCT.

Another issue in this system is the fact that two electronic states contribute to the lowest Born−Oppenheimer (BO) surface that the trajectories run on. Figure 3 shows the two lowest energy diabatic surfaces for $(NO_2-C_2H_2)^+$, cut along the NO_2 bend and symmetric stretch coordinates at infinite $NO_2 - C_2H_2$ separation. The $NO_2^+ + C_2H_2$ reactant state is the global minimum by 1.8 eV; however, because of the difference in equilibrium geometry between NO_2^+ (linear) and NO_2 (134°), there are regions in configuration space where the $NO_2 + C_2H_2^+$ charge state is lower in energy. As reactants approach, the crossing becomes avoided, and the lowest BO surface smoothly connects regions where the electronic configuration corresponds to $NO_2^+ + C_2H_2$ and $NO_2 + C_2H_2^+$. As discussed previously, the charge is roughly equally shared between the reactant moieties in geometries like RC, TS1, or the Ring complex.[1]

There are two concerns here. One is that the QCT code used does not allow for nonadiabatic (surface hopping) transitions at surface crossing seams. Surface hopping would be important if the transition between the two charge states during collisions was abrupt, i.e., if the avoided crossing was localized, with small intersurface splitting, and/or if the motion perpendicular to the seam were rapid. There is no reason to expect any of these conditions to hold. The motion perpendicular to the seam is ONO bending, which is a relatively low frequency motion (54 fs). The transition between $NO_2^+ + C_2H_2$ and $C_2H_2^+ + NO_2$ seems to be smooth, as indicated by the charge on the C_2H_2 moiety during the trajectories (Figure 4). It appears that by the time the collisional interaction is strong enough to distort the system into geometries where $C_2H_2^+ + NO_2$ becomes the dominant configuration, the interaction also has mixed the diabatic states strongly enough to result in gradual transitions.

Another potential problem for systems with avoided crossings is that there might be geometries near the crossing seam where a single reference wave function is inadequate, leading to inaccurate forces in the DFT calculations. We tested for this problem by running single point CASSCF(8,8) calculations for geometries explored by a sample set of trajectories. The coefficient of the Hartree−Fock configuration was greater than 0.95 in all but one geometry, and even there the coefficient was >0.85. Use of a single reference DFT method should not be a serious problem.

IV. Results and Discussion

Before the calculations are presented, it is useful to review the nature and time scales of the motions we are simulating. The time scale of the collisions is somewhat arbitrary, but three numbers are relevant. The time between trajectory start and the onset of strong intermolecular interaction is 80−100 fs, depending on reactant orientation. The time during which the interaction is strong can be hundreds of femtoseconds if the system traps into the five-membered ring complex (Figure 1), but for most trajectories it is in the 50−100 fs range. A more important time period is that between the onset of strong interaction and the point when the first new bond begins to form. This period (30−50 fs) is important because this first bond formation event is at or near the critical point in the collision; thus dynamics occurring after bond formation have no effect on the integral cross section and vibrational enhancements. The classical vibrational periods of the different NO_2^+ modes range from 54 fs for the bend (010) to ~14 fs for the asymmetric stretch (001). The acetylene vibrational periods range from 55 to 9.9 fs. For the levels of excitation relevant for reactants, rotational time scales are tens of picoseconds. It can be seen that vibration is on a time scale comparable to the collision time, while rotational motion is very slow.

Linear NO_2^+ has two degenerate bend modes, corresponding to bending in the $x-z$ or $y-z$ plane, with classical turning point near 167° (i.e., ~13° from linear) for the (010) state (including zero point energy). In the (02^00) state, the bending motion is

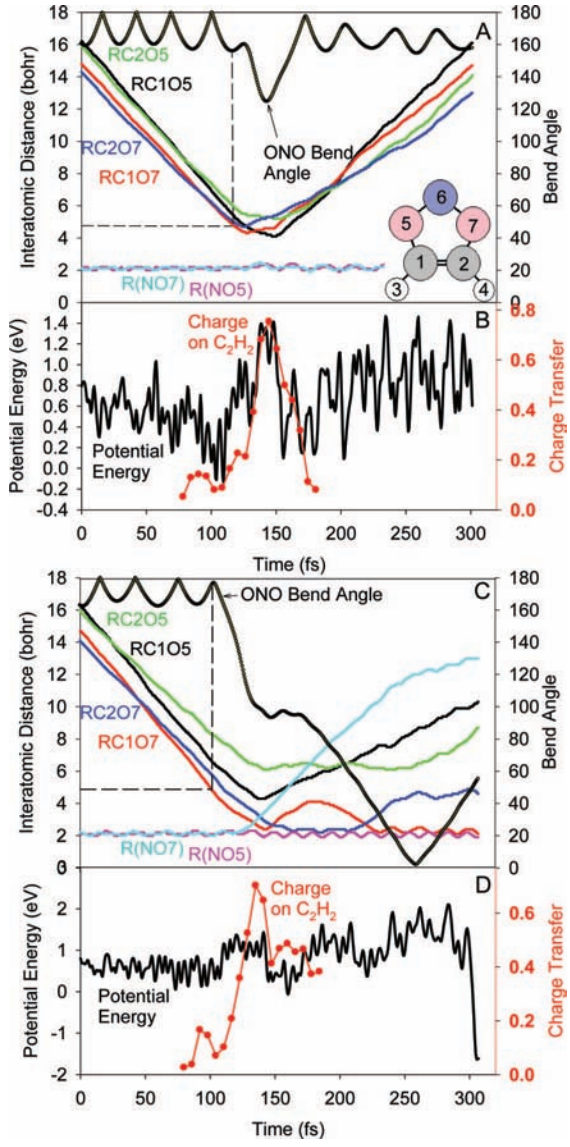

Figure 4. (A) Values of several geometric parameters as a function of trajectory time for a typical nonreactive (02^00) trajectory. The inset (five-membered ring structure) shows the atom numbering. The dashed lines indicate the trigger distance used in most of the analysis (2.5 Å). (B) Potential energy (left scale) and Mulliken charge on the C_2H_2 moiety (right scale). (C and D) Same parameters recorded for a reactive (02^00) trajectory.

also in a single plane, with classical turning point of ~163° (17° from linear). The (02^20) state has one quantum in each of the orthogonal bend planes, 90° out of phase, such that the molecule classically is bent at a fixed angle of ~167°, rapidly "twisting" about what would be the molecular axis in linear NO_2^+. We use the term "twist" for this motion which occurs on a vibrational time scale ($\tau_{twist} \sim 35.4$ fs), to draw the distinction with the usual rotation of NO_2^+ about an axis perpendicular to the molecular axis ($\tau_{rotation} \sim 40$ ps for $J = 1$). From this classical perspective, the relevant differences between the two bend overtone states appear to be as follows: The (02^00) turning point is more bent than the fixed bend angle in the (02^20) state, the (02^00) state explores both linear and bent geometries, and the (02^20) state undergoes a high-frequency twisting motion. The time-averaged bend angle for the two states is quite similar.

A. Typical Trajectories. Before discussing the results in detail, we first will briefly present typical nonreactive and reactive trajectories to illustrate the nature of the motion and

TABLE 1: Trajectory Opacity Functions and Cross Sections. Comparison with Experimental Absolute Cross Sections

impact parameter b (Å)	reactant state		
	GS	02^00	02^20
1.0	0.328	0.397	0.331
1.5	0.265	0.347	0.281
2.0	0.140	0.140	0.140
2.5	0.000	0.000	0.000
σ (Å^2) trajectory	3.16 ± 0.35	3.76 ± 0.36	3.25 ± 0.38
σ (Å^2) expt	2.79	5.36	4.13

changes in energy throughout the collision. Several typical trajectories are presented as mpeg movie files in the Supporting Information for this paper. The top half of Figure 4 summarizes a typical nonreactive trajectory, tracking the ONO bend angle and distances from both O atoms to the N and C atoms as a function of time. The atom numbering scheme used to label the distances is shown in the inset. For example, RNO7 is the distance between the N atom and one of the O atoms, which happens to be atom number 7. Also shown are the potential energy (PE) of the system and the Mulliken charge on the C_2H_2 moiety. The oscillations in the various distances and ONO bend angle during reactant approach reflect the vibrations of the reactants, and it can be seen that the amplitudes are nearly constant during reactant approach, but have changed after the collision, reflecting translation-to-vibrational (T → V) energy transfer. The strong collisional interaction begins at about 120 fs, as indicated by both the PE and collision-induced distortion of the ONO angle. There is substantial transfer of charge to the C_2H_2 moiety during the strongly interacting phase of the collision. There is also a peak in the PE, during this phase of the collision, reflecting the fact that the interaction is predominantly repulsive.

The reactive trajectory shown in the bottom half of the figure is generally similar. In this particular trajectory the transferred O atom (O7) initially bonds to both C atoms forming a three-membered ring (oxirene) structure, which subsequently rearranges to give the ketene product. Again there is substantial charge transfer to C_2H_2 during the collision, but the changes in PE are not so obvious, indicating that the contributions from attractive and repulsive interactions roughly cancel.

B. Trajectory Validation. As discussed above, there are potential problems with the QCT method, and while we can argue that they may not be serious, the best test is how well the trajectories reproduce the experiments. Table 1 gives the calculated opacity functions, $P(b)$, for the three states studied, and compares the resulting cross sections to those measured in the experiments. The error limits given for the trajectory cross sections are statistical, based on the number of trajectories (~970) calculated for each state, and obviously do not include any systematic errors. As discussed above, use of identical pseudorandom initial conditions for each trajectory set should significantly reduce the relative uncertainty in comparing the cross sections for reaction of different NO_2^+ states; however, it is difficult to quantify this reduction.

The uncertainty in the absolute scale of the experimental cross sections was estimated to be 20%, and we estimated that the relative uncertainty in comparing cross sections for difference vibrational states was ~15%. Considering that the cross sections are small, there are no adjustable parameters and that the level of theory is necessarily modest, the agreement with the experimental absolute cross section is quite reasonable—within experimental error for the ground state. The fact that we did

not calculate trajectories for $b = 0.5$ Å or below means that the trajectory cross section is a lower limit; however the effect should be small because such low b collisions are relatively infrequent. As discussed below, reaction at this energy is controlled to a large extent by collision orientation; thus there is no reason to expect that $P(b)$ will increase dramatically at small b. If we assume that $P(b)$ for $b < 1$ Å is similar to the value at $b = 1.0$ Å, then the correction to the cross section from these lower b collisions would be ~15%.

The more important result, in both the trajectories and experiments, is the cross section dependence on NO_2^+ vibrational state. The trajectories show the correct trend for the two excited states, with a greater enhancement for the (02^00) state compared to the (02^20) state. Note, however, that the magnitude of the vibrational enhancements is smaller in the trajectories than in the experiments. This "damping" of the vibrational effects is typical in our experience with QCT studies of vibrational effects,[5,23−25] and we tentatively associate it with the failure to quantize vibrational motion.

The other experimental observation that the trajectories can be tested against is the product recoil velocity distribution. We do not expect QCT to be as accurate in calculating product properties because they are sensitive to accumulation of error throughout trajectories, whereas reactant effects depend only on early time behavior. Experimentally there are two product channels, $NO^+ + C_2H_2O$ and $NO + C_2H_2O^+$, which form in a ~4:1 ratio at high E_{col} but otherwise have nearly identical dynamics, including recoil behavior.[1] The trajectories are only able to probe the major channel, as this corresponds to the lowest Born−Oppenheimer surface. Despite these limitations, it is interesting to see how well the trajectories predict the recoil behavior.

The experiments measured only the projection of the full two-dimensional recoil velocity distribution on the axis of the instrument (the v_{axial} distribution). Because the experiment is cylindrically symmetric, the relative velocity vector of the collisions (v_{rel}) is coincident, on average, with the instrument axis, thus the v_{axial} distribution provides several types of dynamical information. The top frame of Figure 5 shows the experimental v_{axial} distributions for the NO^+ product from reaction of NO_2^+ in its ground and (02^00) states at a nominal collision energy of 2 eV. The distributions are normalized such that the area under each curve is proportional to the integral cross section for that state. Note that the ground-state distribution peaks at positive velocity, corresponding to forward scattering. The peak is quite broad, however, as might be expected if reaction occurred for a range of impact parameters, leading to scattering over a wide angular range from forward (large b) to backward (small b). For the (02^00) state, the growth in signal is mostly in the forward-scattered half of the distribution, which becomes considerably more forward peaked. A similar, but smaller shift to more forward scattering was observed for the (02^20) state. These changes indicate that the vibrational enhancement comes mostly from collisions that result in more strongly forward-scattered products. In fact the peak of the distributions shifts to near the velocity expected for a spectator stripping mechanism (dashed vertical line labeled V_{SS}).

The lower frame of the figure shows the analogous trajectory v_{axial} distributions (lines with data points). generated by adding together the b-weighed distributions calculated from the sets of trajectories at $b = 1$, 1.5, 2, and 2.5 Å (although none of the 2.5 Å trajectories reacted). The area under each curve is proportional to the trajectory integral cross section. The three curves without data points show how each range of impact parameter contributes to the v_{axial} distribution for the ground-state reaction. As expected, as b is increased, the scattering shifts forward. If we had calculated trajectories at $b \leq 0.5$ Å, these presumably would have contributed primarily to the backward-scattered tail, improving agreement with the experimental distributions. The agreement between the trajectories and experiments is not bad, considering the limitations of the calculations. The overall shape of the distributions is reasonably consistent, and the vibrational enhancement comes almost entirely from collisions that lead to forward-scattered products.

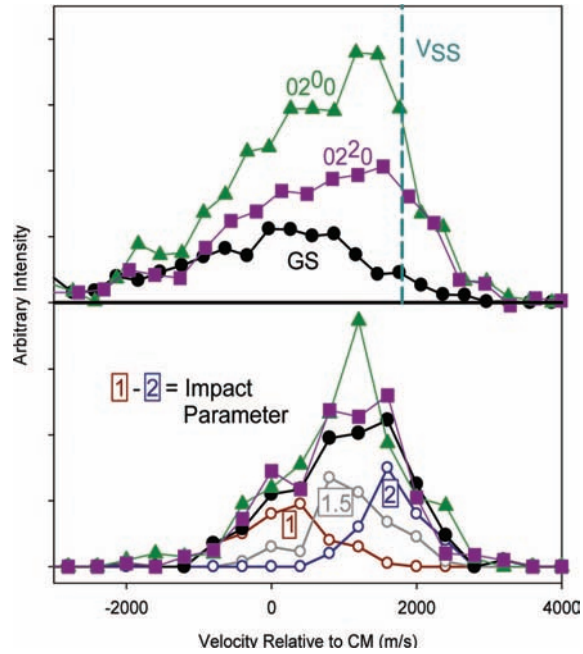

Figure 5. NO^+ product recoil axial velocity distributions at nominal collision energy of 2 eV: (top) experimental, with the spectator stripping velocity indicated as V_{SS}; (bottom) QCT distributions (filled symbols). Also shown are the contributions to the ground-state distribution from different ranges of impact parameter (open symbols).

Note, however, that the trajectories suggest a reinterpretation of the origin of the vibrational effects on reactivity and recoil behavior. The obvious interpretation for a simultaneous increase in reactivity and shift toward more forward-scattered products is that vibrational excitation increases reaction probability at large impact parameters, which tend to scatter forward. Table 1 shows that vibrational excitation, instead, enhances reaction probability at intermediate values of b, with no enhancement at large impact parameters. Instead, the increase in forward-scattered intensity with vibrational excitation in the trajectories results from two changes in scattering behavior for these intermediate b collisions. The angular distribution calculated at $b = 1.5$ Å shifts to smaller scattering angles with vibrational excitation—the peak shifts from ~65° for ground-state NO_2^+ to ~50° for the (02^00) state. In addition, the recoil energy increases with vibrational excitation. Both factors contribute to the shift to higher axial velocities.

In summary, the trajectories correctly predict the absolute cross section magnitude and qualitative trends in cross section versus vibrational state, and even the product scattering is qualitatively right. We, therefore, feel justified in analyzing trajectory details to extract further dynamical insight.

C. Dependence on Bend Angle. One obvious question, given the strong enhancement from bend excitation, is whether reaction probability is a simple function of the bend angle at some critical point in the collision. For low energies the obvious

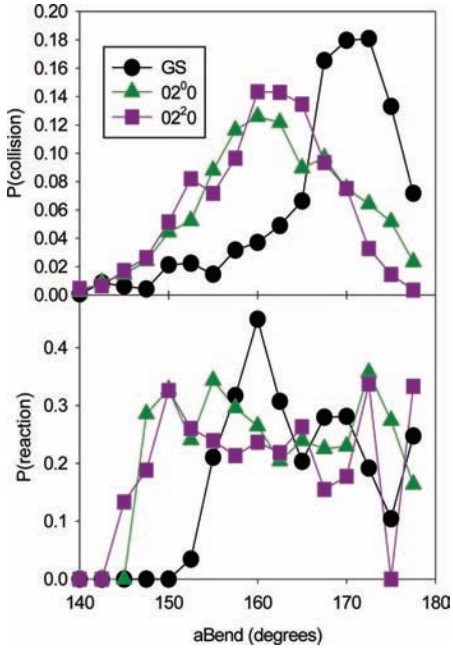

Figure 6. (Top) Distributions of the ONO bend angle (aBend) recorded at the trigger point for the ground, (02^00), and (02^20) states. (Bottom) Reaction probability for trajectories that have different values of aBend at the trigger point.

critical point would be TS1; however, at high E_{col} trajectories do not follow the minimum energy path, and therefore the choice of an event to "trigger" recording the collision geometry is somewhat arbitrary. The ideal trigger should be early enough in the trajectory that collisional forces have not strongly distorted the reactants but late enough that vibration or rotation does not significantly change the geometry in the time between the trigger and the onset of the strong collisional interaction. In past studies we have used the point where the potential energy (PE) first deviates significantly from the range of PE corresponding to zero-point motion of the reactants or when some bond length goes outside the range expected for vibration of the reactants. In this system a wide variety of behavior is seen in the trajectories, and neither method provides a reliable trigger. On the basis of viewing hundreds of trajectories, we have chosen to record the collision geometry for each trajectory at the time step when the shortest CO distance first drops below a particular value. For most of the analysis below, this trigger distance was 2.5 Å, which is typically reached just as collisional distortion of the reactant geometry becomes obvious (see Figure 4, where this trigger distance ($4.7a_0$) is indicated).

The top frame of Figure 6 plots the distributions of the ONO bend angle ("aBend") recorded at the 2.5 Å trigger point for all three states. As expected, the ground state (GS) has a narrower distribution of bend angle, peaking at >170°. The distributions for the (02^00) and (02^20) states are broadened and shifted to smaller angle compared to the ground state (GS), and as expected, the (02^20) distribution does not extend to linear geometries but also peaks at larger aBend than the (02^00) distribution. The small angle tail in the GS distribution, and the breadth of all three distributions, reflect the fact that for this trigger distance, there are some trajectories where collisional interaction has already begun to distort the NO_2^+. Further discussion of bend angle distribution changes with trigger distance is given below.

The lower frame of the figure gives the reaction probability as a function of aBend, i.e., the fraction of reactive trajectories

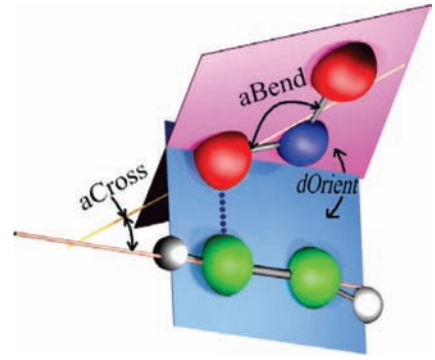

Figure 7. Definition of aCross and dOrient angles.

in each range of aBend, averaged over the impact parameters studied with appropriate weighting. The main conclusion is that reaction probability is at most weakly dependent on NO_2^+ state, and also on aBend, over the ranges of aBend that each state explores. Therefore we cannot rationalize the increase in cross section with bend excitation as simply being due to increased probability of colliding in a bent geometry. It is true that the ground state appears to have a spike in reactivity around 160° (and zero reactivity for aBend ≤150°); however, the number of ground-state collisions in this range of aBend is too small to have much effect on the cross section. Clearly, to understand why the different NO_2^+ vibrational states react with different efficiencies, we need to look further.

D. The Nature of the Bottleneck to Reaction. Before we get further into the details of the molecular motions that enhance and inhibit reaction in this system, it is useful to examine the nature of the bottleneck that controls reactivity. At low E_{col}, RRKM analysis clearly shows that TS1 is the rate-limiting TS and that decay of RC through TS1 can explain the sharp reactivity spike at low energies.[1] TS1 represents a point where CO bonds begin to form, and at low energies reaction is only energetically possible if two CO bonds form concertedly, generating the five-membered ring complex. Distortions away from the C_{2v} TS1 geometry such that only one CO bond can form initially are energetically inaccessible at low E_{col}, and this strong orientation dependence is evidently the cause of the very low reaction efficiency (0.5−2.2% for E_{col} < 1 eV for ground state).

At high E_{col}, the system can react in less symmetric geometries. Indeed, only ~30% of reactive trajectories still go through a five-membered ring intermediate, and even in those, the two CO bonds usually form sequentially. The dominant mechanism involves collisions where only one CO bond ever forms, leading directly to $(NO + C_2H_2O)^+$ products by NO bond scission. The ability to react in collisions where only one O atom needs to interact with one C atom raises the question of whether collision orientation can still account for the fact that reaction efficiency is only ~10% for ground-state NO_2^+ at E_{col} 2 eV. One might imagine that such C−O interactions would occur in a larger fraction of collisions.

It turns out that collision orientation is still a significant controlling factor. One parameter of interest is the angle between what would be the molecular axes of the two reactants, if they were linear at the trigger point. We will call this angle "aCross", and it is indicated on the schematic of the collision geometry in Figure 7.

The top frame of Figure 8 shows the reaction probability for all three states (lines with symbols, left-hand scale), as a function of the value of aCross recorded at the same 2.5 Å trigger point used for the analysis of the aBend dependence of reactivity.

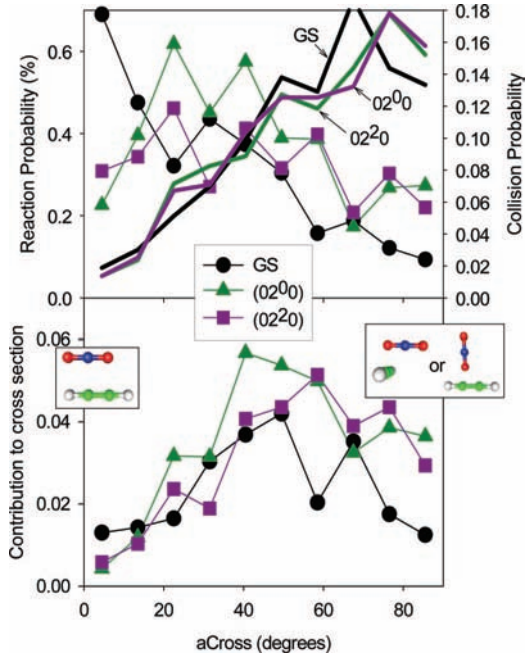

Figure 8. (Top) Curves with symbols (left scale) show reaction probabilities as a function of the aCross angle recorded at the trigger point. Curves without symbols show the probability of trajectories having different values of aCross at the trigger point. (Bottom) The contribution of trajectories in each range of aCross to the reaction cross section.

aCross = 0° corresponds to reactants colliding in a parallel geometry. aCross = 90° describes a range of geometries with the two limiting structures indicated by sketches superimposed on the aCross = 90° axis. For all three states, reactivity generally declines at high aCross, indicating a propensity to react in parallel configurations. The ground-state reactivity peaks at aCross ~ 0°, while the two bend states show peak reactivity for aCross ~15°. Also shown in the top frame of the figure (heavy lines with no symbols, right-hand scale) is the probability of colliding with aCross in a particular angular range (the probability is proportional to sin(aCross), within the statistical uncertainty). The product of the collision probability and reaction probability is the contribution of collisions in each range of aCross to the cross section, and this is plotted in the lower frame of the figure. Note that the differences in reaction probability at small aCross for the different states have no significant effect on the cross section. Instead, it is the higher reaction probability at aCross >30° for the two bend overtone states that has the dominant effect. In any case, it is clear that orientation of the reactants is still an important factor.

Figure 6 showed that ONO bend angle, aBend, was not, by itself, a major factor controlling reactivity. There may be more to this issue, however, because the effect of bend angle may be correlated with other geometric parameters, such that one-dimensional plots such as Figure 6 cannot reveal the dynamics. We examined several two-dimensional correlations of reactivity versus pairs of angles. For example, it seemed likely that aBend might have different effects for collisions in different ranges of aCross; however, within the statistical uncertainty of the trajectory set, the aBend and aCross effects are not correlated.

A more interesting correlation was found between the effects of aBend and a dihedral angle we will call "dOrient" (Figure 7). dOrient describes the orientation of the ONO plane with respect to the plane containing the C_2H_2 CC backbone and the O atom that is attacking it. In essence dOrient tells whether the ONO is oriented such that its O atoms are bent toward the acetylene (small dOrient) or away from the acetylene (large dOrient). Figure 9 shows the correlated distributions of aBend and dOrient for all collisions ("All") and also for only the subset of reactive collisions ("Reactive"). Distributions are given for the three NO_2^+ reactant states and for geometries recorded at a series of trigger distances, defined as described above. First consider the all collisions distributions for ground-state NO_2^+ in the left-most column of the figure. For the 4 Å trigger point, the aBend distribution is, as expected, independent of dOrient within the statistical uncertainty, peaking near 175° and extending to 160°. By the time the trajectories reach the 3.0 Å trigger, there already is some correlation between the two angles, growing quite strong as the reactants approach to smaller separations. The dOrient distribution ultimately splits into two components, indicating that there is a strong torque on ONO orienting its bend plane either parallel or antiparallel to the CC−O plane. One component becomes quite sharply peaked near dOrient = 180° (ONO with the O atoms "bent away" from C_2H_2), and for this component the aBend distribution broadens and shifts to smaller angles (more strongly bent ONO) as the trigger distance decreases. The other component becomes increasingly peaked near dOrient = 0° (ONO with O atoms bent toward C_2H_2), and for this component aBend also broadens and shifts to smaller angles, but less dramatically than for the "bent away" component.

The next column of the figure shows that the "bent away" component is entirely missing in the distribution of reactive collisions, while the "bent toward" component is present with lower intensity than in the all collisions distribution. The implication is that only ONO bent with its O atoms toward C_2H_2 can react and that the reaction efficiency even for this favorable component is less than unity. Note that for all trigger distances, the shapes of this "bent toward" component are quite similar in the distributions of "all" and "reactive" trajectories; i.e., the fraction that reacts is not obviously dependent on the aBend angle.

The middle two columns of the figure show the analogous distributions for all and reactive collisions of NO_2^+ (02^00). At 4.0 Å distance the aBend distribution peaks near 165° and extends from 150° to 180° (i.e., this state inverts through the linear equilibrium geometry). Note that, as expected, the "all collisions" distribution shows no correlation between aBend and dOrient; however, for reactive collisions there is a weak correlation. Trajectories with ONO *bent away* are more reactive when sampled at the 4.0 Å trigger distance. The behavior as the trigger distance is reduced is generally similar to that for ground-state NO_2^+. The distribution splits into two components, with reaction seen only for NO_2^+ which is *bent toward* C_2H_2. The change in reactive trajectories from "bent away" at 4.0 Å to "bent toward" for 2.7 Å and shorter distances reflects the time scale of the collisions. The time it takes reactants to move from 4 to 2.7 Å separation at 2 eV relative energy (~27 fs) is just about half the period of the bend vibration; thus to be bent in the favorable (toward) orientation as the collision begins, the NO_2^+ should be bent away at 4 Å. The one significant difference between the ground state and (02^00) behavior is that trajectories are reactive for the (02^00) state over a wider range of dOrient than for the ground state. This lower sensitivity to orientation is presumably associated with the higher reaction efficiency for this state. It is important to note that the increased range of reactive dOrient is *not* found only for those trajectories where NO_2^+ is more strongly bent at the "moment of collision"—the enhancement is found for the entire range of aBend explored

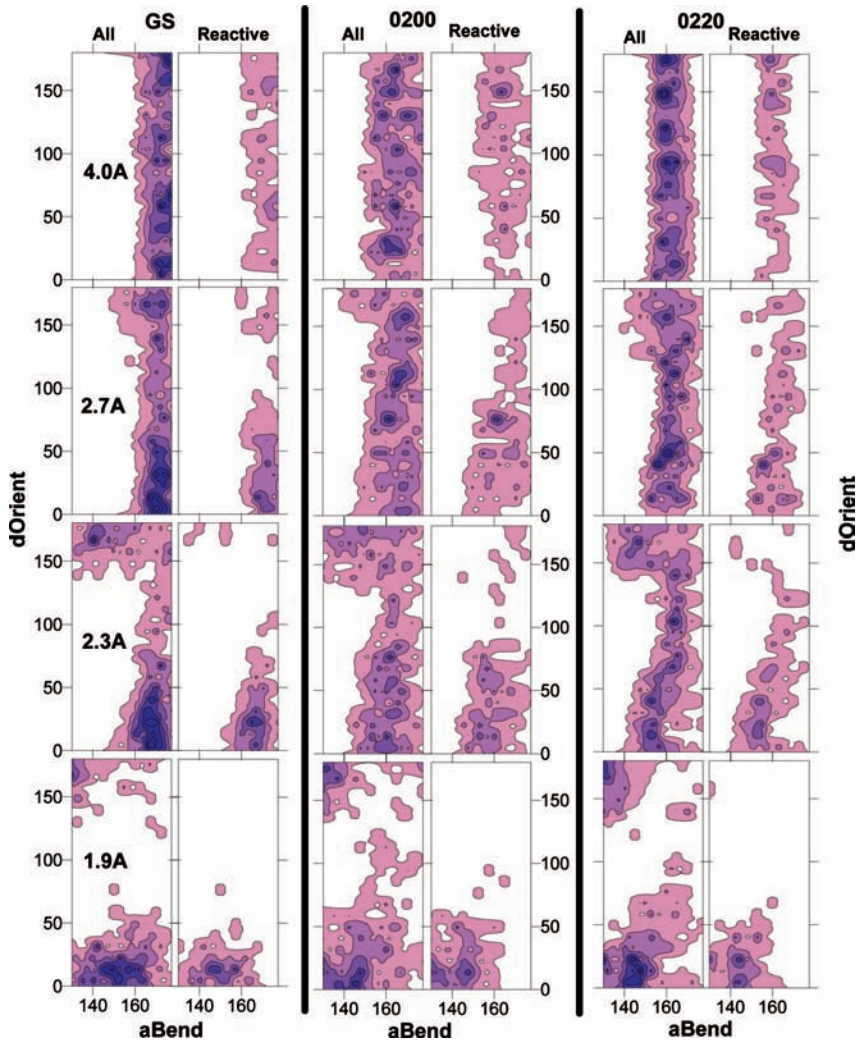

Figure 9. Reactivity vs dOrient (vertical axes) and aBend (horizontal axes) with geometries recorded at four different trigger points (4.0, 2.7 Å, etc., listed in the left column). Results are shown for all trajectories ("All") and for the reactive trajectories ("Reactive") for the ground (GS), 02^20 and 02^00 states.

by the states. It appears that some combination of bending distortion and the momentum associated with the bending motion is responsible for the ability to react in less favorable orientations.

One of the questions we are most interested in is why the (02^20) state is less reactive than the (02^00) state. The right two columns of Figure 9 give analogous aBend/dOrient maps for the (02^20) state. At 4 Å, the aBend distribution for this state peaks at 162° (similar to the (02^00) distribution) but is considerably narrower (155° < aBend < 175°). There is no population at aBend >175°, i.e., this state never samples the linear equilibrium geometry, instead twisting about the linear axis at approximately fixed bend angle (the angle fluctuates somewhat due to zero-point motion). As in the ground state and (02^00) distributions, the reactive trajectories at 4 Å already show some propensity for bending away, switching to a strong preference for bending toward at shorter trigger distances.

The question remains, why the (02^20) state is less reactive than the (02^00) state. Our hypothesis is that the momentum associated with the twisting motion in the (02^20) state makes it difficult for the reactants to remain in the favorable, bent-toward, orientation long enough for the necessary CO bond(s) to form. In essence, this twisting momentum is perpendicular to the reaction coordinate. In contrast, those collisions of the (02^00) state that reach the critical distance (~2.5 Å) in the bent-toward geometry experience no forces that would tend to disturb the orientation. As shown in Figure 9, these reactive trajectories are ones where the vibration has brought the O atom(s) into the favorable orientation just at the point where the forces between C and O atoms begin to be strongly attractive; thus the O atom vibrational momentum reinforces the chemical forces driving CO bond formation.

E. Intracomplex Charge Transfer. In an earlier experimental and trajectory study of NO_2^+ collisional excitation and dissociation in collisions with Kr atoms,[5] it was found that efficient energy transfer was strongly correlated to the degree of transient charge transfer to the Kr moiety during the collision. In all collisions, charge delocalization leads to transfer of at least 40% of the Mulliken charge to the Kr moiety during the strongly interacting phase of the collision. For most collisions, the charge on Kr never exceeds 50%, and there is also very little T → V transfer, and no dissociation even at energies nearly double the dissociation threshold. A small subset of trajectories—those where the NO_2^+ became strongly bent during the collisions—resulted in >80% charge transfer to Kr, and these trajectories ***all*** resulted in large T → V transfer and 100% dissociation. In other words, transient charge transfer to Kr acts as a switch that turns on efficient energy transfer. The mechanism is also obvious in the trajectory results. Both reactants in the NO_2^+ + Kr system are closed shell, but with charge transfer the system

becomes a radical−radical system. Kr^+ attacks NO_2, forms a Kr−O bond, disrupts the NO bonding, and when the charge transfers back the system is left either dissociated or with vibrational excitation above the dissociation threshold. NO_2^+ vibrational excitation enhances the energy transfer/dissociation process, because bending, and to a lesser extent stretching, raises the energy of the $NO_2^+ + Kr$ reactant state and lowers the energy of the $Kr^+ + NO_2$ charge state.

Similar considerations should apply in the $NO_2^+ + C_2H_2$ system. As shown in Figure 3, NO_2^+ vibrational excitation should help drive the system onto the part of the lowest Born−Oppenheimer surface where the charge is transferred to the acetylene reactant, and the $C_2H_2^+ + NO_2$ combination should be substantially more reactive than the closed shell $NO_2^+ + C_2H_2$ reactants. Therefore, it is interesting to look at the degree of charge transfer during collisions and how this correlates with reactivity. A representative set of reactive and nonreactive trajectories was reexamined, with the Mulliken charge calculated at every step during the strongly interacting portion of the trajectory. The fraction of the Mulliken charge appearing on acetylene is shown for a typical pair of trajectories in Figure 4. At least for the set of trajectories examined, it is true that all reactive trajectories involve considerable transient charge transfer during the collision (>60%). On the other hand, some, but not all, nonreactive trajectories also involve substantial intracomplex charge transfer, as shown in Figure 4. That such trajectories are nonreactive is simply the result of the strong dependence of reactivity on dOrient. Many of the trajectories in the "bent away" components (dOrient near 180°) of the "All" collisions distributions undergo substantial charge transfer, resulting in distortion to small ONO angles. None of these trajectories can react, because the O atoms are bent away from the C_2H_2 reactant. The analogous "bent-away" collisions are also unreactive in the $NO_2^+ + Kr$ system, but in addition they also never result in substantial charge transfer, presumably because more extreme distortion of the ONO is required to drive charge transfer in that system because Kr has a much higher ionization energy (14.0 eV) than C_2H_2 (11.4 eV). Kr−O bonding is essential to help drive this extreme distortion, and as a consequence there is a one-to-one correspondence between charge transfer and dissociation. In the present system, the system can be driven into geometries corresponding to charge transfer more easily, thus the correlation between charge transfer and reaction is weakened.

V. Conclusions

Quasi-classical trajectories calculated at the PBE1PBE/6-311G** level of theory are able to reproduce the magnitude of the absolute reaction cross section for oxygen transfer in $NO_2^+ + C_2H_2$. In addition, the QCT results get the dependence of reactivity on NO_2^+ vibrational state and the vibrational state dependent scattering behavior qualitatively correct. Analysis of the trajectories shows that the bending effect is not simply a consequence of enhanced reactivity in bent geometries but, rather, that excitation of bending motion allows reaction in a wider range of orientation angles, even if the NO_2^+ is not bent at the onset of the strongly interacting phase of the collision. The effect is attributed to the fact that bending momentum is coupled to the reaction coordinate for CO bond formation, which is the rate-limiting step in the reaction. The suppressing effect of bending angular momentum is attributed to the fact that its momentum is essentially perpendicular to the CO bond formation coordinate. There is a strong interplay between NO_2^+ bending and transient charge transfer during the collisions. Such charge transfer enhances reactivity, but only if the reactants are oriented correctly.

Acknowledgment. We are grateful to Professor William Hase and Dr. Upakarasamy Lourderaj (Texas Tech University) for developing and providing the VENUS code needed to setup initial conditions for the trajectories, including simulating bending angular momentum. Jack Simons (Utah) provided useful advice on convergence problems at some levels of theory. This work was supported by the National Science Foundation (CHE-0647124).

Supporting Information Available: Videos showing nonreactive and reactive trajectories. This material is available free of charge via the Internet at http://pubs.acs.org.

References and Notes

(1) Boyle, J. M.; Uselman, B. W.; Liu, J.; Anderson, S. L. *J. Chem. Phys.* **2008**, *128*, 114304.
(2) Orr, B. J. *Chem. Phys.* **1995**, *190* (2,3), 261.
(3) Depristo, A. E.; Geiger, L. C. *Surf. Sci.* **1986**, *176* (3), 425.
(4) Clary, D. C. *J. Chem. Phys.* **1981**, *75* (1), 209.
(5) Liu, J.; Uselman, B. W.; Boyle, J. M.; Anderson, S. L. *J. Chem. Phys.* **2006**, *125*, 133115/1.
(6) Kreher, C.; Theinl, R.; Gericke, K.-H. *J. Chem. Phys.* **1996**, *104* (12), 4481.
(7) Liu, J.; Van Devener, B.; Anderson, S. L. *J. Chem. Phys.* **2005**, *123* (20), 204313/1.
(8) Liu, J.; Van Devener, B.; Anderson, S. L. *J. Chem. Phys.* **2004**, *121*, 11746.
(9) Liu, J.; Devener, B. V.; Anderson, S. L. *J. Chem. Phys.* **2003**, *119*, 200.
(10) Kim, H.-T.; Green, R. J.; Anderson, S. L. *J. Chem. Phys.* **2000**, *113*, 11079.
(11) Kim, H.-T.; Green, R. J.; Anderson, S. L. *J. Chem. Phys.* **2000**, *112*, 10831.
(12) Green, R. J.; Kim, H.-T.; Qian, J.; Anderson, S. L. *J. Chem. Phys.* **2000**, *113*, 4158.
(13) Qian, J.; Green, R. J.; Anderson, S. L. *J. Chem. Phys.* **1998**, *108*, 7173.
(14) Fu, H.; Qian, J.; Green, R. J.; Anderson, S. L. *J. Chem. Phys.* **1998**, *108*, 2395.
(15) Qian, J.; Fu, H.; Anderson, S. L. *J. Phys. Chem.* **1997**, *101*, 6504.
(16) Anderson, S. L. *Acc. Chem. Res.* **1997**, *30*, 28.
(17) Chiu, Y.-H.; Fu, H.; Huang, J.-T.; Anderson, S. L. *J. Chem. Phys.* **1996**, *105*, 3089.
(18) Liu, J.; Uselman, B.; Van Devener, B.; Anderson, S. L. *J. Phys. Chem. A* **2004**, *108*, 9945.
(19) Lourderaj, U.; Martinez-Nunez, E.; Hase, W. L. *J. Phys. Chem. A* **2007**, *111* (41), 10292.
(20) Hase, W. L. Bolton, K. de Sainte Claire, P. Duchovic, R. J. Hu, X. Komornicki, A. Li, G. Lim, K. Lu, D. Peslherbe, G. H. Song, K. Swamy, K. N. Vande Linde, S. R. Varandas, A. Wang, H. and Wolf, R. J. *VENUS99: A general chemical dynamics computer program*, 1999.
(21) Bakken, V.; Millam, J. M.; Schlegel, H. B. *J. Chem. Phys.* **1999**, *111*, 8773.
(22) Frisch, M. J.; Trucks, G. W.; Schlegel, H. B.; Scuseria, G. E.; Robb, M. A.; Cheeseman, J. R. ; Montgomery J. A., Jr.; Vreven, T.; Kudin, K. N.; BurantJ. C. Millam, J. M.; Iyengar, S. S.; Tomasi, J.; Barone, V.; Mennucci, B.; Cossi, M.; Scalmani, G.; Rega, N.; Petersson, G. A.; Nakatsuji, H.; Hada, M.; Ehara, M.; Toyota, K.; Fukuda, R.; Hasegawa, J.; Ishida, M.; Nakajima, T.; Honda, Y.; Kitao, O.; Nakai, H.; Klene, M.; Li, X.; Knox, J. E.; Hratchian, H. P.; Cross, J. B.; Bakken, V.; Adamo, C.; Jaramillo, J.; Gomperts, R.; Stratmann, R. E.; Yazyev, O.; Austin, A. J.; Cammi, R.; Pomelli, C.; Ochterski, J. W.; Ayala, P. Y.; Morokuma, K.; Voth, G. A.; Salvador, P.; Dannenberg, J. J.; Zakrzewski, V. G.; Dapprich, S.; Daniels, A. D.; Strain, M. C.; Farkas, O.; Malick, D. K.; Rabuck, A. D.; Raghavachari, K.; Foresman, J. B.; Ortiz, J. V.; Cui, Q.; Baboul, A. G.; Clifford, S.; Cioslowski, J.; Stefanov, B. B.; Liu, G.; Liashenko, A.; Piskorz, P.; Komaromi, I.; Martin, R. L.; Fox, D. J.; Keith, T.; Al.Laham, M. A.; Peng, C. Y.; Nanayakkara, A.; Challacombe, M.; Gill, P. M. W.; Johnson, B.; Chen, W.; Wong, M. W.; Gonzalez, C.; Pople, J. A. *Gaussian03*; Gaussian, Inc: Wallingford, CT, 2004.
(23) Liu, J.; Song, K.; Hase, W. L.; Anderson, S. L. *J. Phys. Chem. A* **2005**, *109*, 11376.
(24) Liu, J.; Song, K.; Hase, W. L.; Anderson, S. L. *J. Am. Chem. Soc.* **2004**, *126*, 8602.

(25) Liu, J.; Song, K.; Hase, W. L.; Anderson, S. L. *J. Chem. Phys.* **2003**, *119*, 3040.

(26) *CRC Handbook of Chemistry and Physics*; Weast, R. C., Astle, M. , Beyer, W. H., Eds.;CRC Press: Boca Raton, FL, 1985.

(27) Chantry, P. J. *J. Chem. Phys.* **1971**, *55*, 2746.

(28) Press, W. H.; Teukolsky, S. A.; Vetterling, W. T.; Flannery, B. P. *Numerical Recipies in C. The Art of Scientific Computing*, 2nd ed.; Cambridge University Press: Cambridge, 1992.

(29) Laaksonen, L. gOpenMol (available at www.csc.fi/gopenmol/, Espoo, Finland, 2002).

(30) Miller, W. H.; Hase, W. L.; Darling, C. L. *J. Chem. Phys.* **1989**, *91* (5), 2863.

(31) Untch, A.; Schinke, R.; Cotting, R.; Huber, J. R. *J. Chem. Phys.* **1993**, *99*, 9553.

JP8101404